Supporting Information:

Subsurface Imaging of Cell Organelles by Force Microscopy

*Carlos R. Guerrero‡, Pablo D. Garcia‡ and Ricardo Garcia**

Instituto de Ciencia de Materiales de Madrid, CSIC,

c/ Sor Juana Ines de la Cruz 3, 28049 Madrid, Spain

* Email: r.garcia@csic.es.

‡These authors contributed equally to this work.

List of contents

Experimental details and force-distance curves

The experimental steps to obtain force-distance curves (FDC) from the AFM observables are described in Fig. S1. The tip is approached towards the cell from an initial tip height (Fig. S1a). By determining the contact point, the actual tip-sample distance is deduced (Fig. S.1b). Negative tip-sample distances mean that the tip is indenting the cell (Fig. S1c). From cantilever deflection curve, the force-distance curve is obtained by multiplying it with the cantilever force constant (Fig. S1e). Fig. S1e shows a typical FDC obtained on a NIH-3T3 fibroblast. Far from the cell, the approach and retraction tails of the FDC do not coincide (Fig. S1f). This is due to the hydrodynamic drag of the cantilever. The drag force has been corrected (Fig. S1g) by applying the method described in ref. 1[1].

Supporting Figure 2 shows a collection of FDC taken, respectively, on the nucleosol, nucleoli, actin star and cytoplasm areas of two NIH-3T3 fibroblasts.

The reproducibility the method has been verified by imaging other NIH-3T3 cells. The images are shown in Supplementary Figures 3 and 4.

Nanomechanical and optical images of nuclear organelles

To determine that the viscosity coefficient maps enable the imaging of nuclear structures, in Fig. S5 we compare the topography, viscosity coefficient and optical phase contrast images of two cells. The agreement obtained between the features observed by optical phase contrast and the viscosity coefficient images inside the nucleus confirms the subsurface features of the method. Fig. S5 shows that subsurface features cannot be observed in the AFM topography images.

Finite element simulations

We include some finite element method simulations (FEM) to estimate the influence of the actin bundle thickness on the measured Young's modulus. FEM simulations also provide insight on the dependence of the Young's modulus with the density of fibers.

SUPPORTING INFORMATION FIGURES

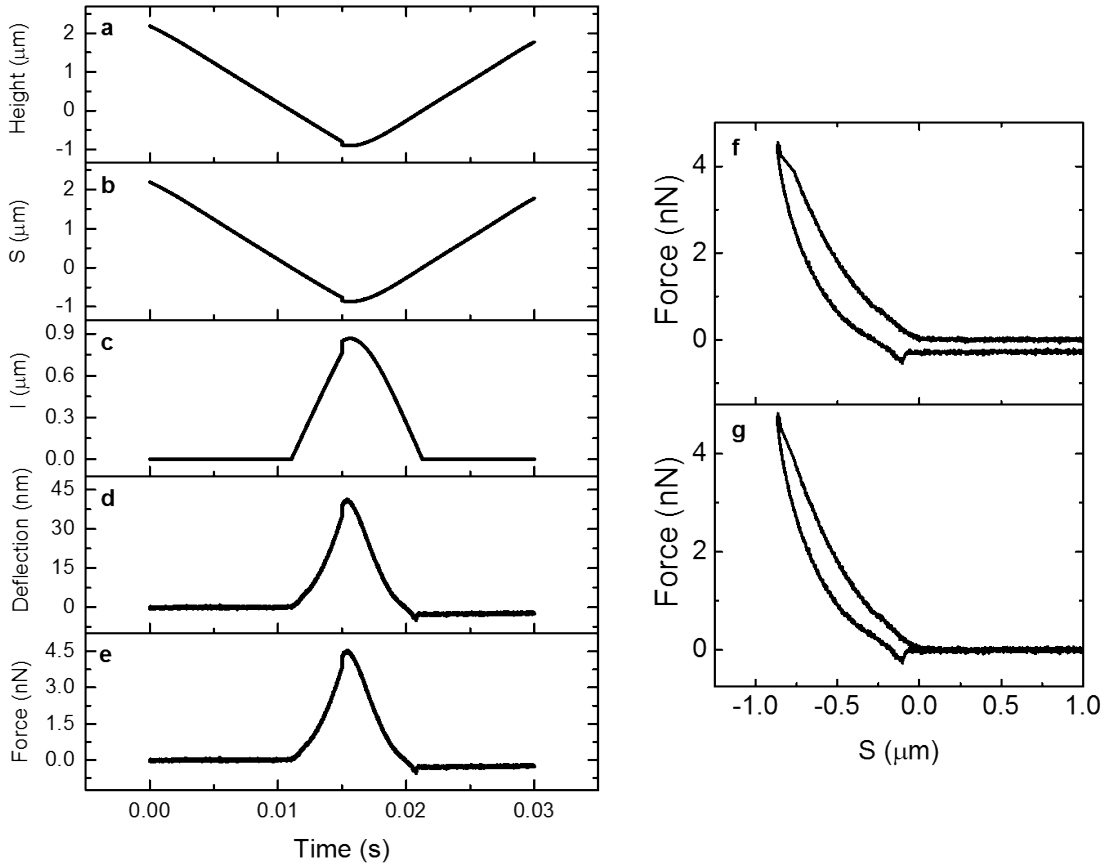

Supporting Figure 1. Steps to generate a FDC on a living cell by approaching the tip towards the cell with a triangular wave form. (a) Tip height versus time. (b) Tip-sample distance. (c) Indentation. (d) cantilever deflection. (e) Force versus time. (f) FDC obtained on a NIH-3T3 fibroblast before hydrodynamic drag correction. (g) FDC resultant after hydrodynamic drag correction.

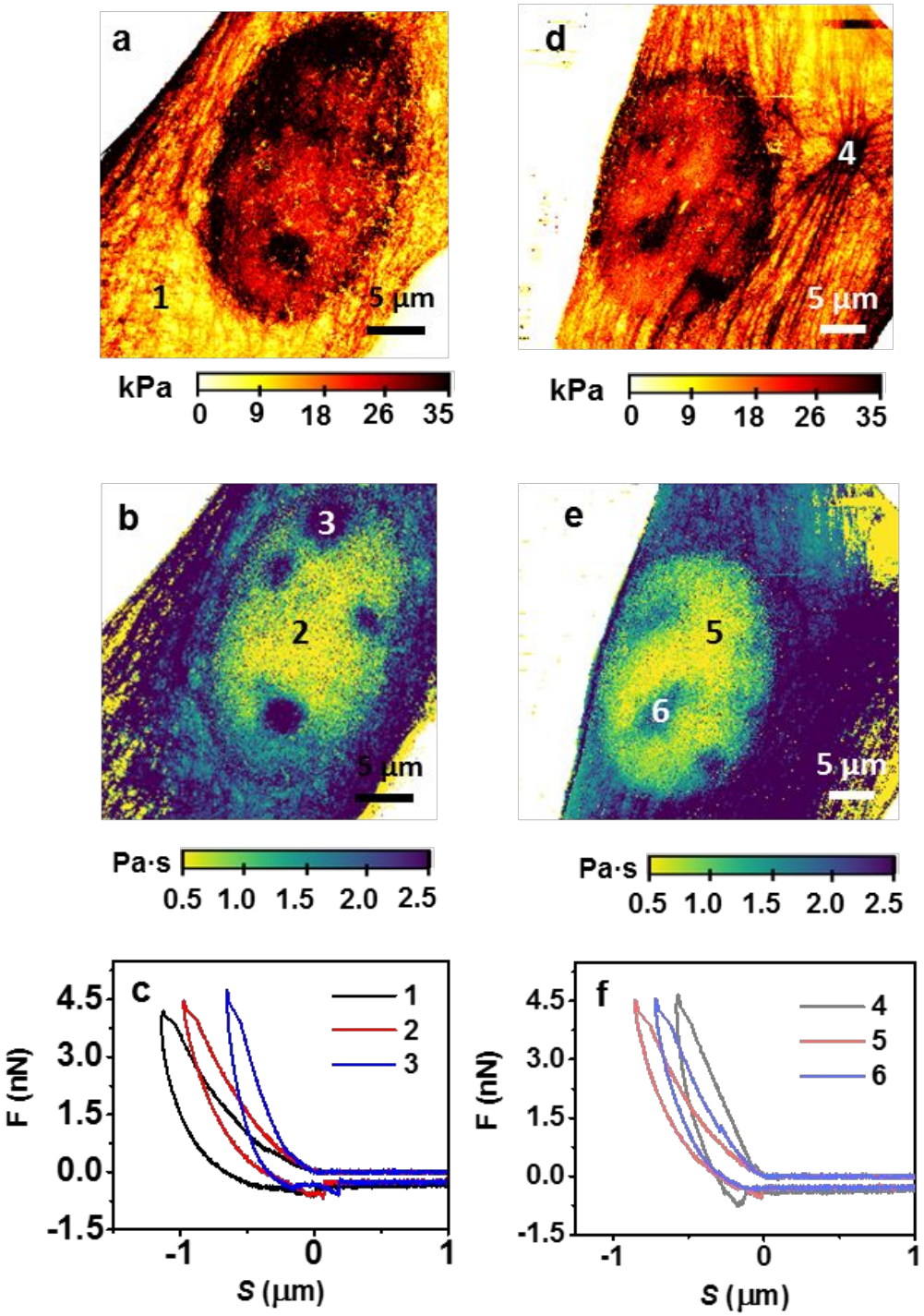

Supporting Figure 2. Examples of experimental FDC taken on different locations of two NIH-3T3 cells. (a) Young's modulus map of a cell. (b) Viscosity coefficient map. (c) Force-distance curves on the point marked in panels a and b. (d) Young's modulus map of a cell. (e) Viscosity coefficient map. (f) Force-distance curves on the point marked in panels d and e.

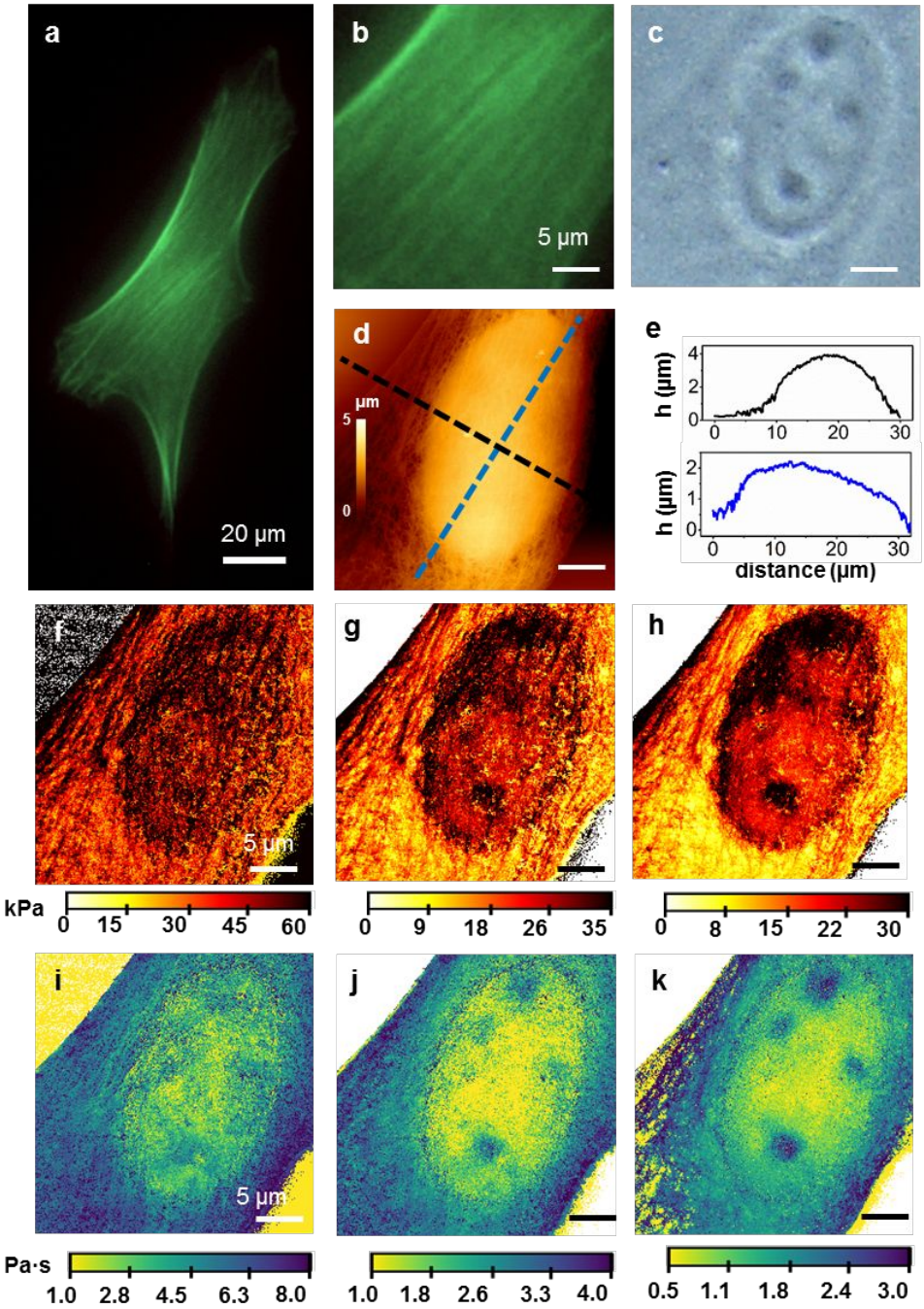

Supporting Figure 3. (a). Fluorescence image of the actin cytoskeleton of a NIH 3T3 fibroblast. (b). Zoom from a. (c). Optical phase contrast image of the region shown in b. (d). AFM height image of the region shown in panels (b-c). (e). Height cross-sections along the dashed lines marked in (d). (f). Young's modulus map for ΔI=50-200 nm. (g). Young's modulus map for ΔI=200-400 nm. (h). Young's modulus map for ΔI=400-850 nm. (i). Viscosity coefficient map for ΔI=50-200 nm. (j). Viscosity coefficient map for

ΔI=200-400 nm. (h). Viscosity coefficient map for ΔI=400-850 nm. These maps shows several organelles inside the nucleus.

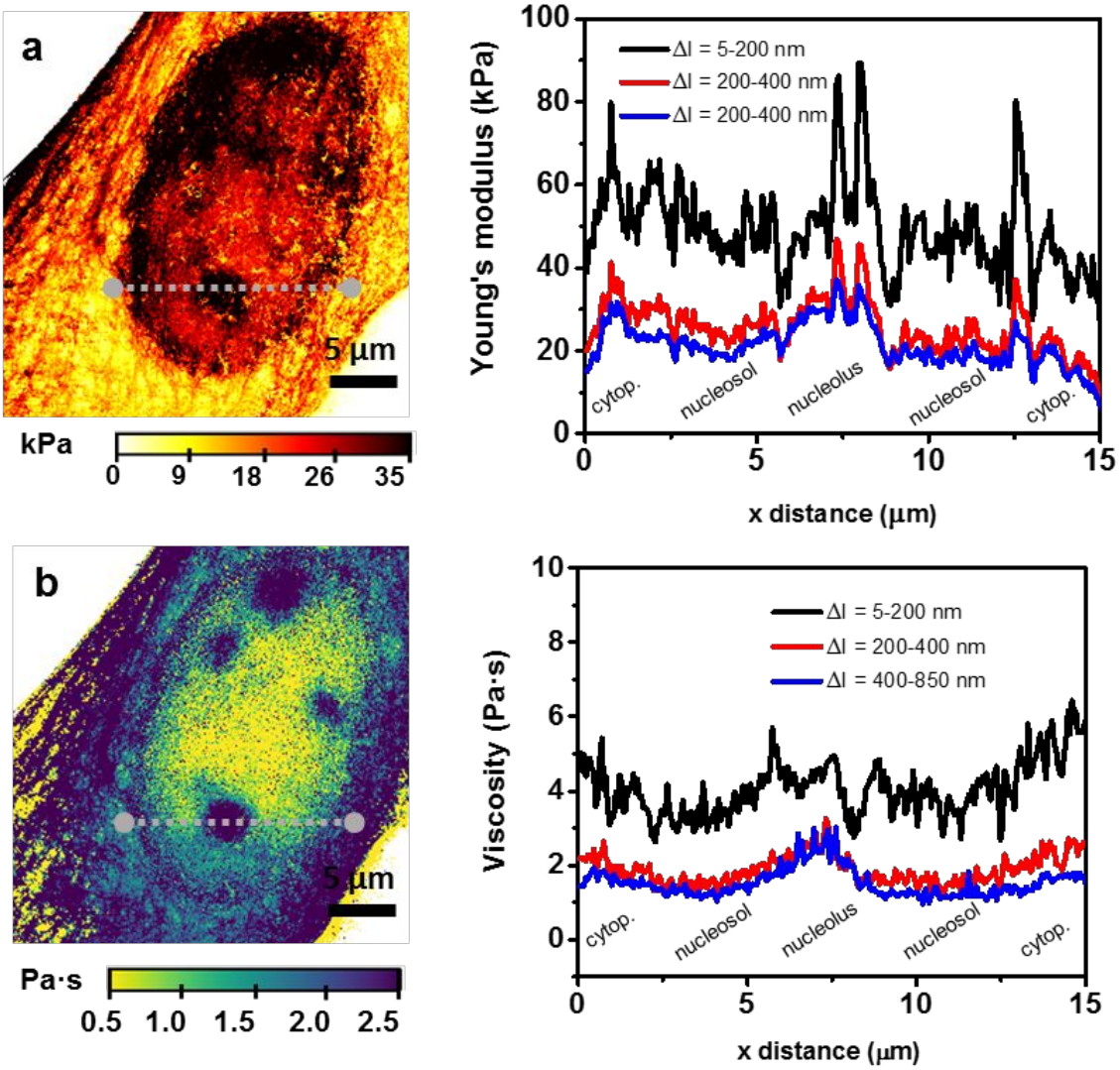

Supporting Figure 4. (a). Young's modulus map (left) and the cross-sections across the line marked on the map. The cross-sections have been extracted from panels (f-h) shown in Fig. S3. (b). Viscosity coefficient map and the cross-sections across the line marked on the map. The cross-sections have been extracted from panels (i-k) in Fig. S3.

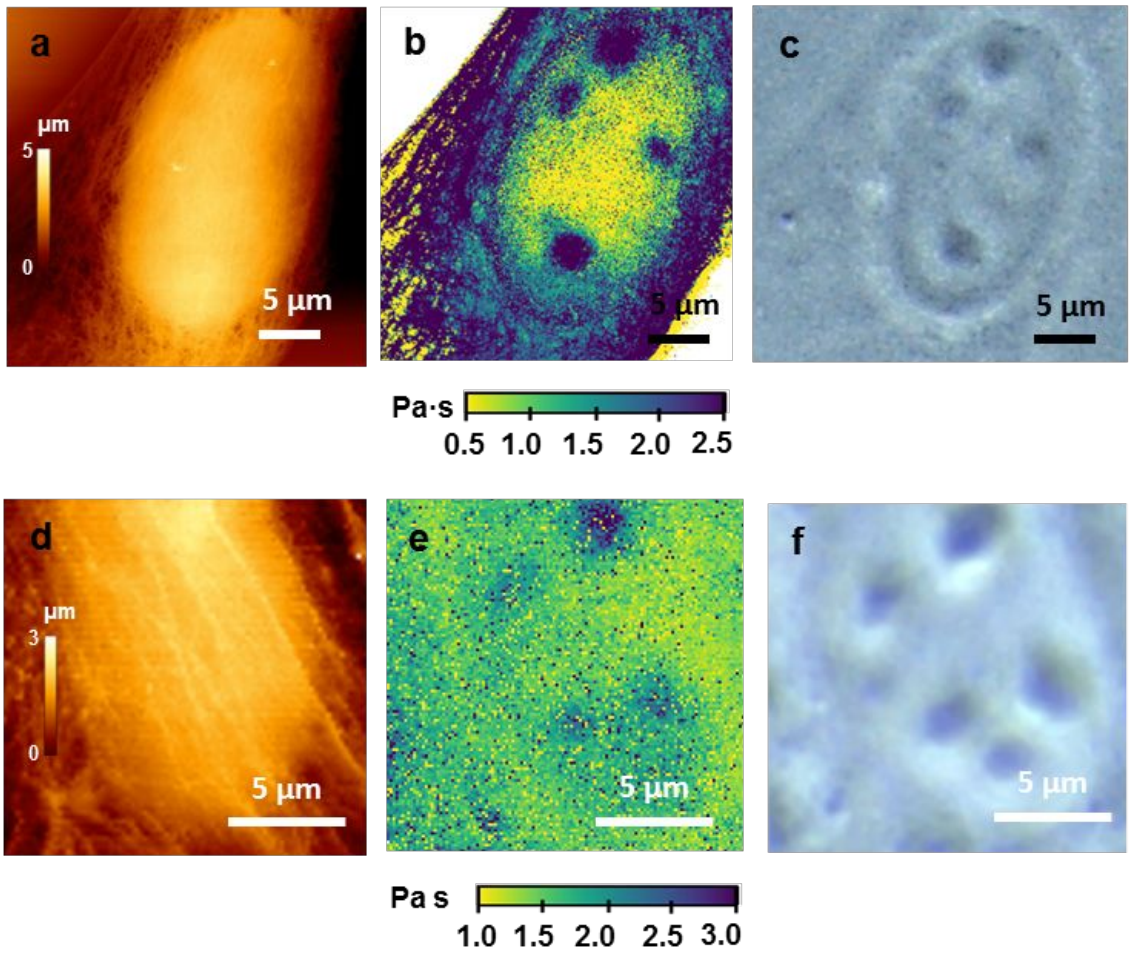

Supporting Figure 5. Comparison between AFM images and optical images of nuclear organelles. (a). AFM height image (topography) of a fixed fibroblast cell. (b) Viscosity coefficient map of the cell shown in (a). (c) Optical phase contrast image of the cell shown in (a). (d). AFM height image (topography) of a live fibroblast cell. (e) Viscosity coefficient map of the cell shown in (d). (f) Optical phase contrast image of the cell shown in (d).

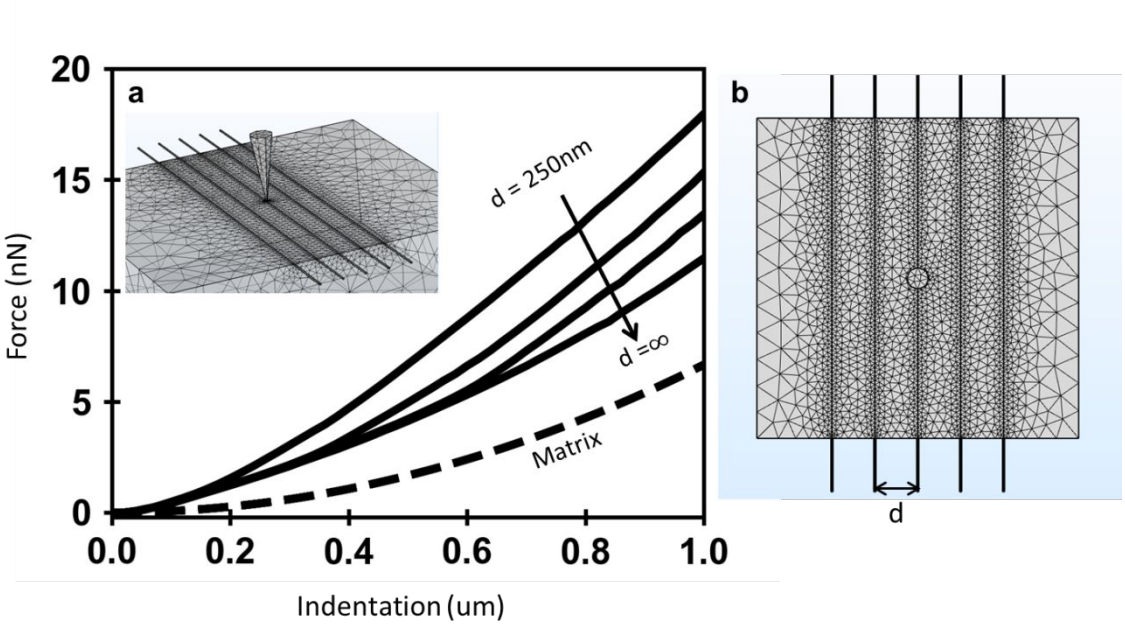

Supporting Figure 6. Force-distance curves by FEM simulation for an array of fibers placed on the surface of an elastic matrix. (a) Scheme of the tip-sample system. (b) Force-distance curves as a function of the separation among fibers. FEM data: Young's module: fiber 1 GPa, matrix= 4 kPa; tuip with a d half-cone angle of 70º.

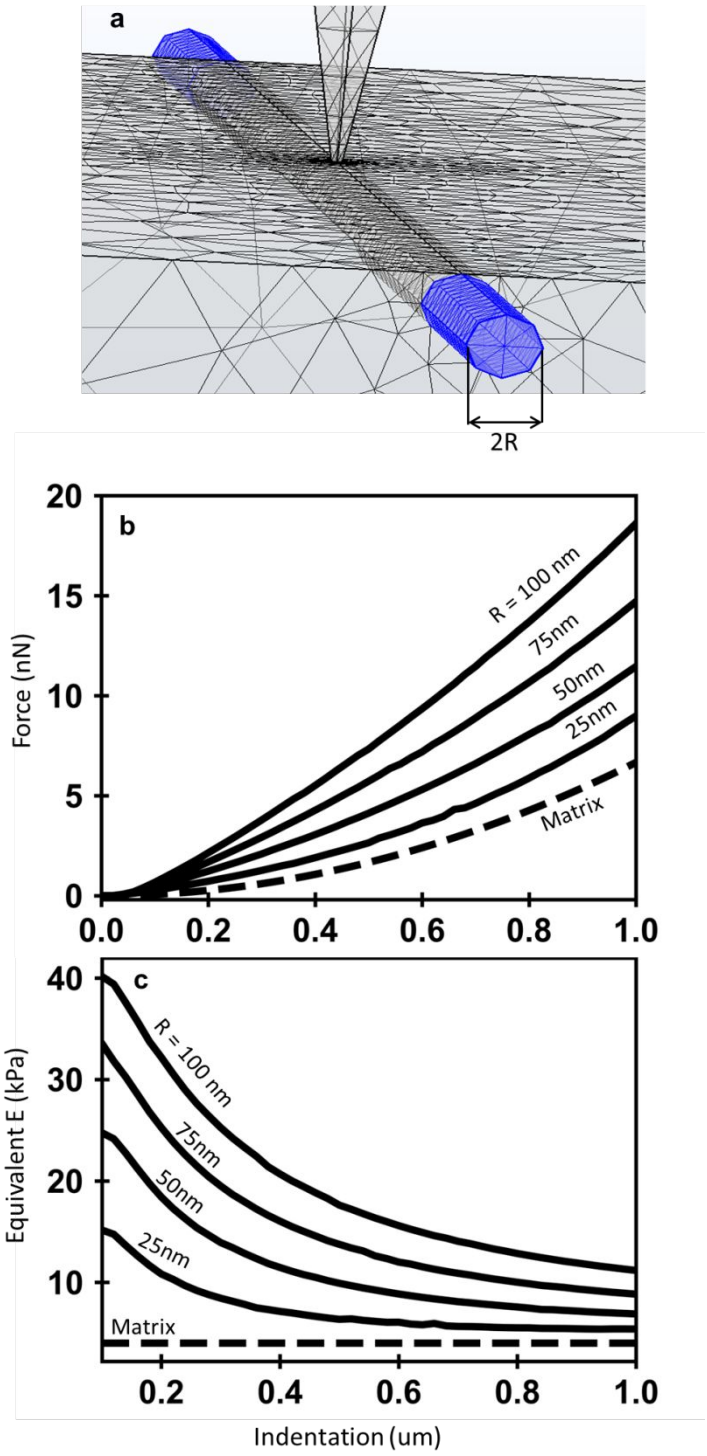

Supporting Figure 7. (a) Scheme of the FEM simulation. (b) Force-distance curves as a function of the fiber diameter. (c) Effective Young's modulus for the different fibers. FEM data: Young's module: fiber 1 GPa, matrix= 4 kPa; tip with a d half-cone angle of 70º.

Supporting references

(1) Garcia, P. D.; Guerrero, C. R.; Garcia, R. Time-Resolved Nanomechanics of a Single Cell under the Depolymerization of the Cytoskeleton. *Nanoscale* **2017**, *9*, 12051–12059.